



HAL
open science

Structure and reactivity with oxygen of $\text{Pr}_2\text{NiO}_{4+\delta}$: an in situ synchrotron X-ray powder diffraction study

Thibault Broux, Carmelo Prestipino, Mona Bahout, Serge Paofai, Erik Elkaim, Vaibhav Vibhu, Jean-Claude Grenier, Aline Rougier, Jean-Marc. Bassat, Olivier Hernandez

► To cite this version:

Thibault Broux, Carmelo Prestipino, Mona Bahout, Serge Paofai, Erik Elkaim, et al.. Structure and reactivity with oxygen of $\text{Pr}_2\text{NiO}_{4+\delta}$: an in situ synchrotron X-ray powder diffraction study. Dalton Transactions, 2016, 45 (7), pp.3024-3033. 10.1039/c5dt03482e . hal-01259407

HAL Id: hal-01259407

<https://univ-rennes.hal.science/hal-01259407>

Submitted on 26 Feb 2021

HAL is a multi-disciplinary open access archive for the deposit and dissemination of scientific research documents, whether they are published or not. The documents may come from teaching and research institutions in France or abroad, or from public or private research centers.

L'archive ouverte pluridisciplinaire **HAL**, est destinée au dépôt et à la diffusion de documents scientifiques de niveau recherche, publiés ou non, émanant des établissements d'enseignement et de recherche français ou étrangers, des laboratoires publics ou privés.

*Structure and reactivity with oxygen of Pr₂NiO_{4+δ}: an
in situ synchrotron X-ray powder diffraction study*

Thibault Broux¹, Carmelo Prestipino^{1*}, Mona Bahout¹, Serge Paofai¹, Erik Elkaïm², Vaibhav Vibhu³, Jean-Claude Grenier³, Aline Rougier³, Jean-Marc Bassat³, Olivier Hernandez^{1*}

¹ Institut des Sciences Chimiques de Rennes (ISCR), Equipe « Chimie du Solide et Matériaux », UMR CNRS N°6226, Université de Rennes 1, 263 Avenue du Général Leclerc, 35042 RENNES, France

² Synchrotron SOLEIL, L'Orme des Merisiers, Saint-Aubin - BP 48, 91192 GIF-SUR-YVETTE Cedex, France

³ CNRS, Université de Bordeaux, ICMCB, UPR 9048, F-33608 PESSAC, France

Abstract

The promising SOFC cathode material $\text{Pr}_2\text{NiO}_{4+\delta}$ has been studied *in situ* under pure oxygen by high resolution synchrotron X-ray powder diffraction. The room temperature (RT) average crystal structure turns out to be monoclinic. The subtle monoclinic distortion ($\gamma = 90.066(1)^\circ$ at RT) is elucidated and further interpreted in terms of specific tilt schemes of the NiO_6 octahedra. It is also shown that $\text{Pr}_2\text{NiO}_{4+\delta}$ is incommensurately structurally modulated already at room temperature, in the manner of the homologous cobaltate $\text{La}_2\text{CoO}_{4.14}$. On heating, the phase transition to the High Tetragonal Temperature (HTT) phase is completed at 480°C without any evidence for the Low Temperature Orthorhombic phase allowing clarifying the phase diagram of this K_2NiF_4 -type ternary oxide. Moreover, it turns out that above 800°C the HTT phase transforms reversibly in two coexisting isomorphous tetragonal phases. The incommensurate modulation is surviving up to 950°C , although modified concomitantly with the two abovementioned phase transformations. Additionally the role of kinetics on the decomposition process is highlighted through new thermo-gravimetric analyses.

Introduction

The main scientific challenge in the field of SOFC (Solid Oxide Fuel Cell) materials is to lower the operating temperature (typically $T < 800$ °C), as it offers several benefits in long term operation such as decreasing the instability at the interfaces^{1, 2} and reducing the starting time and the fabrication cost. To reach such objective, the replacement of lanthanum strontium manganite – the most common cathode material – is mandatory due to its loss of performance at operating temperature lower than 800 °C³. In this scope mixed ionic-electronic conductors (MIECs) are promising for the development not only of SOFCs but more generally of many environmental-friendly electrochemical devices⁴. New generations of SOFC cathodes operating at intermediate temperature require good performances in terms of catalytic activity towards oxygen reduction, electronic conductivity and also ionic diffusivity in the temperature range between 600 and 800 °C. Using MIEC cathodes allows improving the charge transfer kinetics by enlarging the area of the interface between fuel gas, electrode and electrolyte, the so-called triple-phase boundary.

In this context rare-earth nickelates of formula $A_2NiO_{4+\delta}$ ($A = La, Nd, Pr$)^{5, 6} have been widely studied as potential MIEC cathode materials for intermediate temperature SOFC due to their high oxide ion conductivity as well as good compatibility with electrolytes suitable over this temperature range⁶⁻¹². The rare-earth nickelates, and more generally their iso-structural cuprate and cobaltate counterparts, were largely studied in the 90's for their low temperature electronic transport and magnetic properties, such as high temperature superconductivity. Those ternary oxides belong to the series $n = 1$ of the Ruddlesden-Popper (R-P) family ($A_{n+1}M_nO_{3n+1}$), the so-called K_2NiF_4 -type structure. This layered structure is composed by an alternating stack of one

MO_2 perovskite-type layer, within which MO_6 octahedra are corner-sharing, with $(AO)_2$ rock salt bilayers. In the ‘ideal’ or high temperature tetragonal (HTT) structure – corresponding to a perfect matching between perovskite and rock salt layers – MO_6 octahedra are aligned along the stacking direction. However on cooling orthorhombic and tetragonal phases appear with different tilting schemes. K_2NiF_4 -type oxides are well known to be (or to become readily) over-stoichiometric in usual preparation conditions due to their tendency to accommodate interstitial oxygen (O_{int} , located within the rock salt layers), charge compensated by electron holes localized on the transition metal cation M . Their high ionic conductivity results from a diffusion pathway between apical (O_{ap}) and interstitial oxygen atoms through the so-called interstitially mechanism^{7, 13-15}.

In the $A_2NiO_{4+\delta}$ series, $Pr_2NiO_{4+\delta}$ exhibits the highest oxygen diffusion and surface exchange coefficients¹². A peculiarity of this compound lies in the small ionic radius of the Pr^{3+} lanthanide, inducing structural strains within the “PrO” rock salt layers, which results in particularly strong structural distortions with regard to the ideal HTT structure and in the ability to uptake a significant level of oxygen excess to release these strains. However the upper high temperature range, corresponding to the operating conditions of SOFC cathodes, shows controversial results concerning the meta-stability of $Pr_2NiO_{4+\delta}$ in oxidizing atmosphere.

We undertook the *in situ* re-investigation of the high temperature structural properties of $Pr_2NiO_{4+\delta}$ by taking advantage of the high resolution, counting statistics and accessible Q -range obtained on powder diffraction beam lines at third generation synchrotron radiation facilities. An experimental set-up incorporating a zirconia sensor was used in order to accurately control the oxygen partial pressure, pO_2 , within the capillary sample holder. *In situ* synchrotron X-Ray Powder Diffraction (XRPD) data, completed by TGA data, will allow revisiting the phase changes under

oxygen for this promising SOFC cathode material thanks to the detection of subtle structural features.

Experimental

Synthesis

Polycrystalline $\text{Pr}_2\text{NiO}_{4+\delta}$ was synthesized via a high temperature solid-state route. Appropriate ratio of pre-calcinated Pr_6O_{11} and NiO, all of high-purity grade (99.9 % Alfa Aesar for Pr_6O_{11} and 99.99 % Aldrich for NiO), were mixed and ground in acetone. The obtained powder was pelletized and annealed at 1350 °C for 7 h in air and slowly cooled down to RT at 3 °C·min⁻¹. Three annealing with intermediate grindings were necessary to obtain pure composition and high crystalline quality.

As synthesized $\text{Pr}_2\text{NiO}_{4+\delta}$ was characterized at room temperature in air using a Bruker AXS D8 Advance X-ray powder diffractometer equipped with a Ge (111) Johansson-Guinier focusing monochromator and a silicon strip Lynxeye detector. The sample was evaluated as a single phase and indexed in the orthorhombic symmetry. The oxygen over-stoichiometry estimated by iodometric titration performed under a constant argon flow¹⁶ resulted in a δ value equal to 0.22(1).

Scanning electron microscopy (SEM) was performed using a JEOL JSM-6301F confirming a large sized particle (above 2 μm , see Fig. S1) as expected for highly crystalline compounds obtained by ceramic synthesis. Thermo-gravimetric analyses (TGA) were performed using a NETZSCH STA 449F3 thermal analyser on 100 mg of sample in oxygen with a flux of 40 ml/min.

***In situ* synchrotron X-ray powder diffraction**

Synchrotron XRPD data were collected at SOLEIL on the CRISTAL beamline, using the 2-circle diffractometer (capillary Debye-Scherrer geometry) and its high resolution set-up. A wavelength of 0.5113 Å was selected from the natural beam of the undulator through a double-Si monochromator. Detection is performed by 21 Si(111)-crystal analysers followed by fast YAP(Ce) scintillation detectors (Scionix) mounted on each analyser. For each data collection, 21 independent patterns are obtained, which are shifted and summed-up to give the final diffraction pattern measured up to $Q_{max} = 9.8 \text{ \AA}^{-1}$. A minimum FWHM of $0.00346(3)^\circ 2\theta$ was obtained from a NIST LaB₆ pattern.

A reactivity cell that allows various gases to pass through the sample in a quartz capillary with $\varnothing = 0.7 \text{ mm}$ was used in an oscillating mode to ensure a good averaging over the different crystallites. Quartz wool was put in place at the outlet-side of the capillary in order to avoid any ejection of the powder. A Cyberstar hot gas blower was used to reach a maximum temperature of 950 °C on the sample. The investigated sample was studied *in situ* upon heating under two different flowing gas (pressure: 1 bar; output: 100 ml/min): pure oxygen and pure argon, corresponding to the following oxygen partial pressures: 1 and 10^{-3} bar.

All data were analysed by the Rietveld method with the Rietan-FP program¹⁷ using a Toraya split pseudo-Voigt peak shape function. Few isolated reflections broadened anisotropically were subject to a relaxation profile. The background approximated by a finite sum of Legendre polynomials was refined with 12 parameters and an absorption correction (Ida's procedure¹⁸) was applied using a $\mu \times r$ value of 2.6. At RT the occupancy of O_{int} was constrained to the value estimated by iodometric titration and at higher temperature to the values deduced from the TGA. Anisotropic Atomic Displacement Parameters (ADPs) have been used for Pr, Ni and O_{ap} for all temperatures. In the low temperature phase both O_{eq} sites were refined isotropically while in the

HTT phase the single O_{eq} site was refined anisotropically. O_{int} was refined isotropically at all temperatures but in the low temperature phase its U_{iso} was restrained to the value of O_{eq1} . Such an approximation has been validated by the results of the titration-constrained refinement at RT.

The microstructural effects were specifically studied (see Figs. S2-S3) with the FullProf program¹⁹ using the Thompson-Cox-Hastings pseudo-Voigt profile function and the integral breadth method in order to obtain volume averages of sizes and strains. Anisotropic size broadening is modelled using the Scherrer formula that considers the size broadening can be written as a linear combination of spherical harmonics. The anisotropic strain broadening is described using the Stephen's model²⁰. The instrumental resolution function was determined by a Le Bail refinement against a LaB_6 pattern.

For the sake of comparison, in this study all the phases are reported using the same F -setting for the unit cell, consequently space group $I4/mmm$ (N°139) and $C12/m1$ (N°12) will be described in the non-conventional settings $F4/mmm$ (transformation matrix $((1,1,0),(1,-1,0),(0,0,-1))$)²¹ and $F112/m$ (transformation matrix $((1,0,2),(1,0,0),(0,1,0))$).

Results and discussion

Structural characterization at room temperature of $Pr_2NiO_{4.22}$

Although the earlier studies of Willer & Daire²² and Singh *et al.*²³ suggested a monoclinic symmetry for Pr_2NiO_4 , and the previsions by Ganguly and Rao in 1984 a monoclinic structure on the basis of bond distance considerations²⁴, in all the following studies the crystal symmetry assignment of $Pr_2NiO_{4+\delta}$ was limited to orthorhombic $Bmab$ ^{25, 26}, $Pccn$ ²⁷, tetragonal $P4/ncm$ ²⁸⁻³⁰ and orthorhombic $Fmmm$ ^{29, 30} space groups, depending of δ value and temperature. The first three

space groups are associated with systematic tilts of NiO₆ octahedra while the last one is associated with a disordered pattern of octahedra tilts³¹⁻³³. Moreover, to our knowledge, Pr₂NiO_{4+δ} with δ > 0.20 has never been investigated by high resolution synchrotron XRPD. The high angular resolution of this setup (instrumental broadening Δ*Q* ranging from 1.7×10⁻³ to 3.6×10⁻³ Å⁻¹) allows detecting subtle pseudo-symmetry or modulation effects that could be missed by laboratory XRPD or by Neutron Powder Diffraction (NPD).

As shown in Figure 1, the high resolution synchrotron pattern of Pr₂NiO_{4.22(1)} recorded at RT over a large *d*-spacing range (up to *d*_{min} ≈ 0.64 Å) is characterized by narrow reflections revealing a remarkable crystalline quality. Although at first sight the diffraction pattern is roughly similar to the one expected for the *Fmmm* LTO phase, reflections *hhl* turn out to be clearly split as visible for the (220) peak in the inset (b) of Figure 1. As a consequence, a small monoclinic distortion within the *ab* plane must be considered in order to explain the observed splitting of the (*hhl*) reflections. Other formally possible assumptions than a monoclinic distortion for explaining such a splitting (coexistence of two phases, other orthorhombic unit cells...) were ruled out by our exhaustive indexing/Rietveld analyses as well as by the thermal evolution of the XRPD pattern (see below). Therefore, the RT phase of Pr₂NiO_{4+δ} should be named LTM (Low Temperature Monoclinic) instead of LTO.

Three space groups are compatible with the observed cell metric and systematic extinctions: *C121* (N°5); *C1m1* (N°8) and *C12/m1* (N°12). Between those three possibilities, the more symmetric *C12/m1* (with setting *F112/m*), subgroup of the space group *Fmmm* describing disordered K₂NiF₄-type LTO phases, was chosen to build the structural model. Thus it is here implicitly assumed the crystallographic structure of Pr₂NiO_{4.22(1)} to be basically the same as that of the *Fmmm* average model, but with a monoclinic distortion through the loss of the two mirror

planes perpendicular to the a and b axes. This symmetry loss generates only the splitting of the $Fmmm$ equatorial oxygen site (O_{eq} , $1/4, 1/4, 0$ Wyckoff position $8e$) into two non-equivalent positions: $(1/4, 1/4, 0)$ and $(-1/4, 1/4, 0)$, corresponding to the Wyckoff sites $4c$ and $4d$ respectively, while the other sites in $Fmmm$ remain unchanged.

As visible in the Rietveld plot (Figure 1), such a structural model (Table 1) associated with the unit cell $a = 5.39747(14)$, $b = 5.45340(7)$, $c = 12.44140(4)$ Å; $\gamma = 90.0660(12)^\circ$, is adapted to well reproduce experimental data. However, as shown in the inset (a) of Figure 1, still few peaks of minor intensity remain un-indexed, although clearly visible. Such reflections are compatible neither with the metric of the F -centred monoclinic unit cell nor with one of its multiple. Moreover the monoclinic model proposed³⁴ for the homologous compound $\text{La}_2\text{NiO}_{4.25}$, (space group $C2$, $a = 13.832$, $b = 10.930$, $c = 10.912$ Å and $\beta = 113.31^\circ$, four times larger than the orthorhombic unit cell), was not able to index all the above mentioned super-lattice peaks. Hence, those un-indexed reflections should be ascribed to another phenomenon such as an incommensurate structural modulation, probably associated with an ordered tilt scheme of the NiO_6 octahedra and/or an occupational modulation of interstitial oxygen atoms (O_{int}) as proposed previously by Allançon *et al.*²⁸ or by analogy to our previous study on isostructural $\text{La}_2\text{CoO}_{4.14}$ ³².

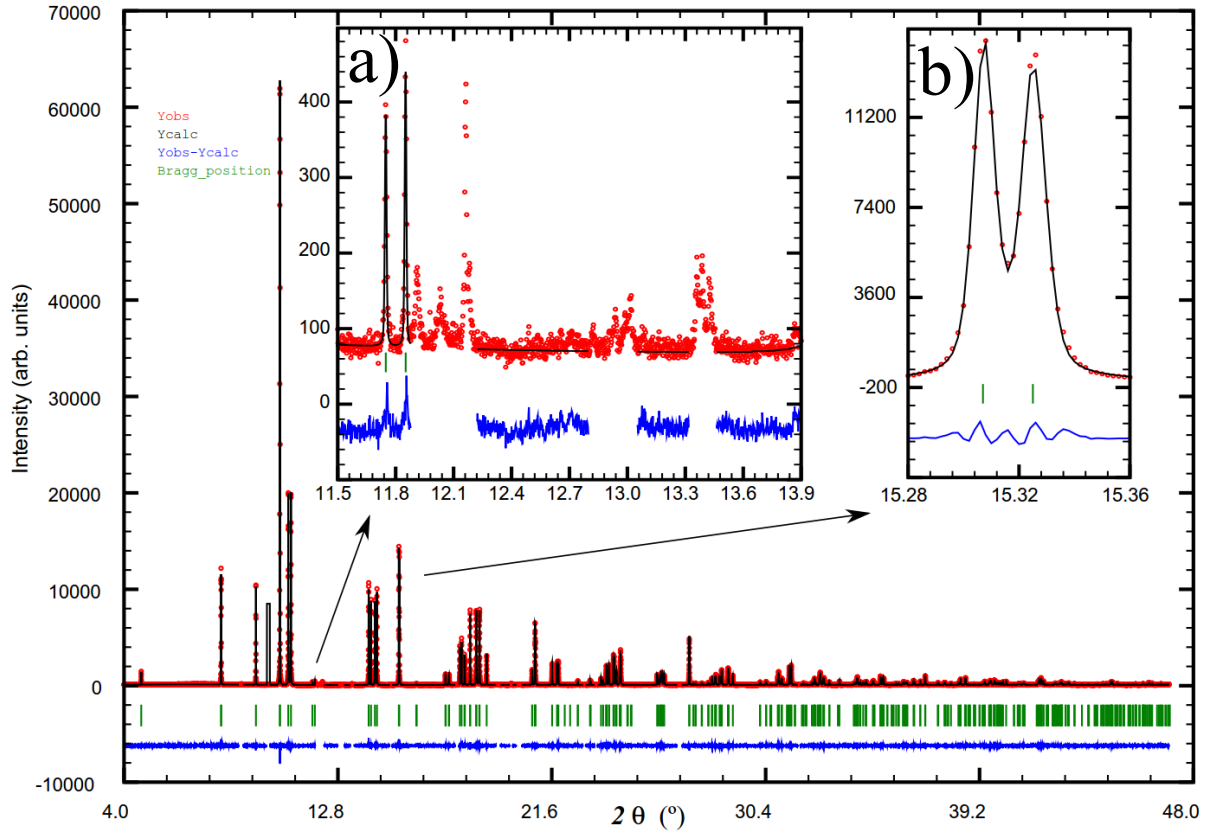


Figure 1. Rietveld plot of $\text{Pr}_2\text{NiO}_{4.22(1)}$ at RT using the $F112/m$ space group. **(a)** Example of unindexed super-lattice peaks. **(b)** Split (-220) and (220) reflections indexed with the space group $F112/m$.

The monoclinic structural model directly deriving from the classical LTO phase is able to reproduce the observed Bragg peak intensities of the $\text{Pr}_2\text{NiO}_{4.22(1)}$ pattern, regardless of the weaker satellite reflections that were excluded during the Rietveld analysis. The structural origin of the observed monoclinic distortion with regard to the $Fmmm$ LTO phase is thus expected to be extremely small.

Starting from the $Fmmm$ model, the building unit most likely affected by a monoclinic distortion is the NiO_6 octahedron that changes from point group D_{4h} (axially elongated octahedron)

to point group D_{2h} due to the loss of degeneracy of the Ni-O bonds along the [110] and [1-10] directions caused by the 0.1% compression along [110]. From an atomistic point of view, such a deformation is not straightforwardly justifiable due that it does not affect significantly neither the electronic levels of Ni nor the strain between perovskite and rock salt layers. The origin of the monoclinic distortion should also be investigated taking care of all structural observables, *i.e.* also the inspection of the values of the ADPs.

From Rietveld analysis (see Table 1), apical oxygen atoms exhibit a very diffuse ellipsoid with a maximum mean square displacement of 0.12 \AA^2 directed along the vector $u = 0.22$, $v = 0.98$ and $w = 0.00$ in fractional coordinates. At RT the origin of a so high ADP for apical oxygen O_{ap} is not thermal but possibly due to two kinds of static distortion: the tilt of octahedra releasing the strain between perovskite and rock salt layers²⁴ and the steric repulsion with interstitial oxygen O_{int} . In the same time equatorial oxygen atoms O_{eq} resulted in two significantly different U_{iso} : $0.014(1)$ and $0.026(2) \text{ \AA}^2$ for sites O_{eq1} ($-\frac{1}{4}, \frac{1}{4}, 0$) and O_{eq2} ($\frac{1}{4}, \frac{1}{4}, 0$), respectively.

Table 1. Structural parameters of $\text{Pr}_2\text{NiO}_{4.22(1)}$ at RT. Space group: $F112/m$. Unit cell parameters: $a = 5.39747(14)$, $b = 5.45340(7)$, $c = 12.44140(4) \text{ \AA}$; $\gamma = 90.0660(12)^\circ$. $R_{wp} = 8.266$, $R_p = 5.879$, $R_{Bragg} = 2.029$, $R_F = 1.622\%$ and $S = 1.3145$. Interstitial oxygen occupancy fixed at the value obtained by iodometric titration and $U_{iso}(O_{int.})$ constrained to the value of $U_{iso}(O_{eq1})$.

Atom	x/a	y/b	z/c	$U_{aniso \text{ or } iso} (\text{\AA}^2)$	Occupancy
Pr	0	0	0.35933(2)	$U_{11} = 0.0112(1)$, $U_{22} = 0.01571(2)$ $U_{33} = 0.00925(9)$, $U_{12} = -0.00122(4)$	1
Ni	0	0	0	$U_{11} = 0.0051(3)$, $U_{22} = 0.00639(3)$ $U_{33} = 0.0158(3)$, $U_{12} = 0.0000(3)$	1
O_{ap}	0	0	0.1737(2)	$U_{11} = 0.055(3)$, $U_{22} = 0.121(4)$ $U_{33} = 0.012(2)$, $U_{12} = 0.015(3)$	1
O_{eq1}	0.25	0.75	0	0.014(1)	1
O_{eq2}	0.25	0.25	0	0.026(2)	1

O _{int} .	0.25	0.75	0.25	0.014(1)	0.11
--------------------	------	------	------	----------	------

Having a close look at ADPs values relatively to the unit cell axes suggest some hypotheses about the origin of the monoclinic distortion (Figure 2b). The longest principal axis of displacement ellipsoid for apical oxygen is at first glance almost oriented along the [010] axis. Such an observation suggests that the main octahedra tilts are similar to those encountered in the *Bmab* LTO phase. To support this statement, the *b* axis is elongated with respect to the *a* one due to the deformation of the O_{eq}-Ni-O_{eq} “scissor” angle, generating a strong orthorhombic splitting³⁵. However, this *Bmab*-based model (that does not justify the observed crystal monoclinic distortion) is compatible neither with the different U_{iso} values of the two non-equivalent equatorial oxygen atoms, nor with the small but significant component along [100] of the longest principal axis of apical oxygen ellipsoid (see Figure 1 b)). The *Bmab* space group describes ordered cooperative tilts around the *a* axis while the *F112/m* one implies no ordering of the octahedra tilts, regardless of a possible modulated structure (see below).

Such features could be explained by superimposing a second scheme of tilts in which NiO₆ octahedra rigidly tilt along the [110] axis. In this tilt scheme, previously proposed by Ganguly *et al.*²⁴ but never experimentally observed, the rigid tilt along [110] shifts equatorial oxygen atoms away from the $z = 0$ plane and the projection of the Ni-O bond along the [110] axis is decreased. The monoclinic distortion in Pr₂NiO_{4.22(1)} is the result of the difference of *d* spacing between the (1 1 0) and (1 -1 0) crystallographic planes (see Figure 2(c)). It is worth to underline that tilts around the O_{eq}-Ni-O_{eq} axis are expected due to the high amount of interstitial oxygen: indeed as calculated for iso-structural La₂NiO_{4+δ}^{36, 37}, O_{int} shifts the four neighbouring O_{ap} along the bond of about 0.5 Å (see Figure 2a red stick) inducing a substantial tilt of the octahedra. This general mechanism

based on the value of the covalent radius for O^{2-} anion is retained for all K_2NiF_4 type oxides, as the matter of fact the HTT structure proposed by Allançon *et al.*²⁸ for $Pr_2NiO_{4+\delta}$ shows the same NiO_6 octahedra preferential tilts around the $O_{eq}-Ni-O_{eq}$ axis, although in such a case the tilting arrangement was ordered and the metric of the unit cell was tetragonal.

It is worth reminding that, although the monoclinic model depicted here implies no long range order of octahedra tilt, the presence of satellite reflections may be related to the position of oxygen atoms and consequently would describe an incommensurate long range order of octahedra tilt with respect to the average monoclinic periodicity. All the attempts to index the observed very weak satellites using the K_Search program of the FullProf suite¹⁹ remain unsuccessful. Solving such a structural modulation, which is likely to be as complex as the one observed in homologous $La_2CoO_{4.14}$ with two independent incommensurate wave vectors^{31, 32}, turns out to be beyond the possibilities of the present powder diffraction study.

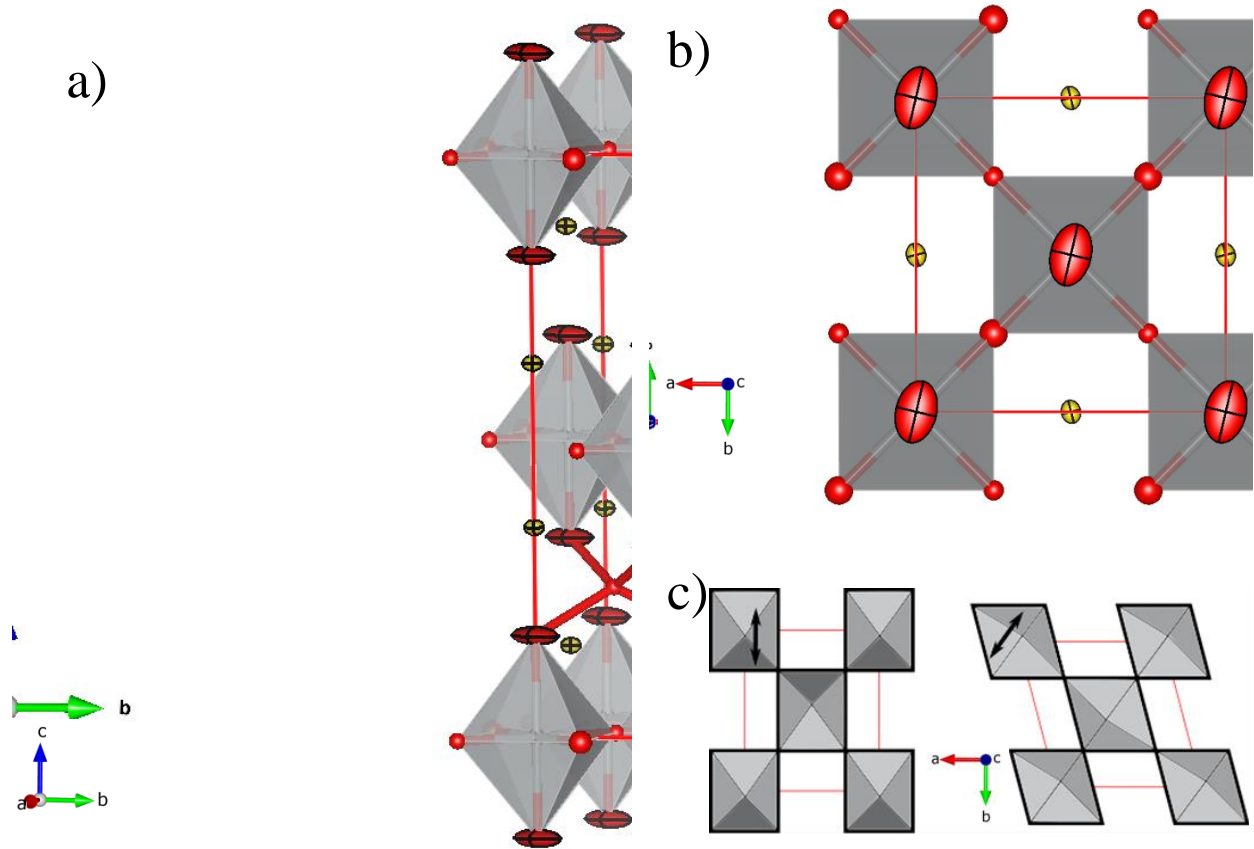


Figure 2. Part a): Unit cell representation of $\text{Pr}_2\text{NiO}_{4.22(1)}$ at RT. Part b) view along the *c* axis evidencing ADP orientation within the *a, b* plane. Ellipsoids are shown at the 50% probability level. Part c) schemes of octahedra tilts at the origin of the orthorhombic and monoclinic distortions (left and right, respectively). It is worth to precise that in part c) the models are representative of a single local arrangement of tilting, no long range order of the tilting can be proposed at this stage.

Thermogravimetric analyses under O₂

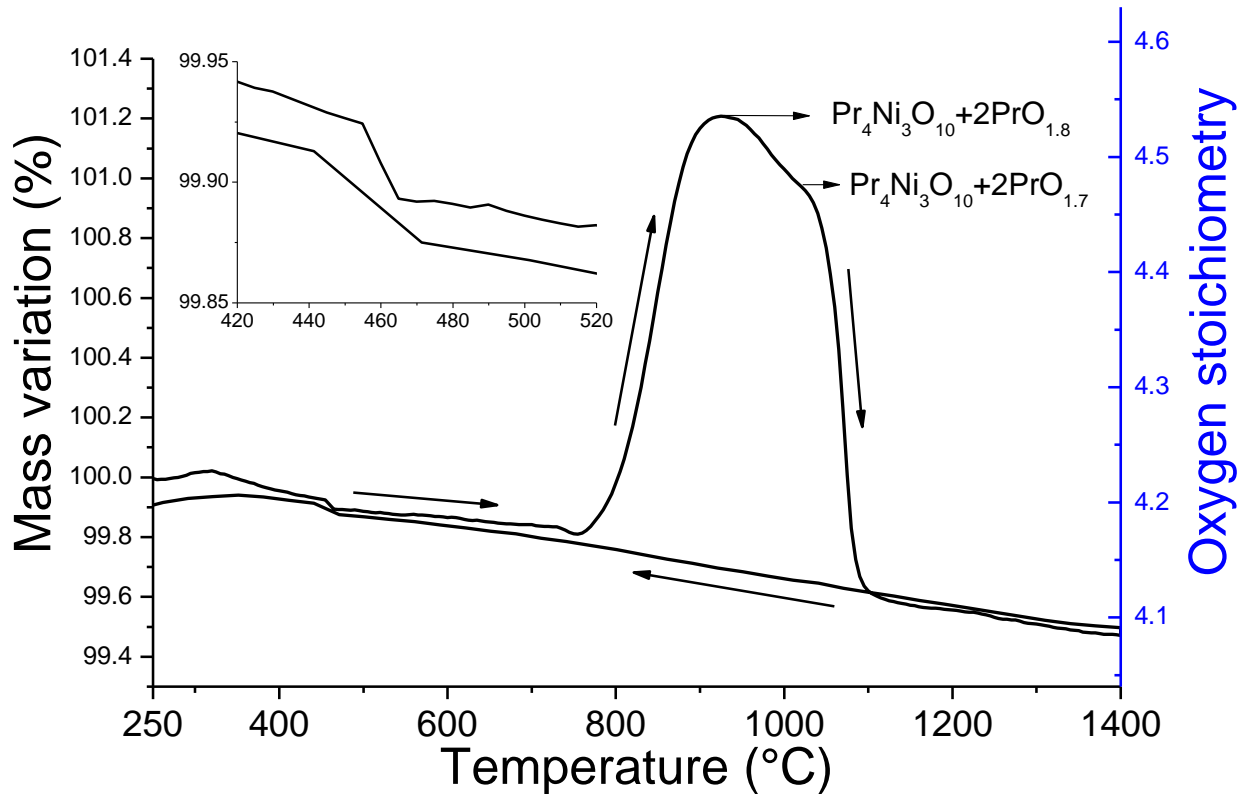


Figure 3. TGA of $\text{Pr}_2\text{NiO}_{4.22}$ performed under O_2 : heating rate $0.5\text{ }^\circ\text{C}/\text{min}$, isotherm at $1400\text{ }^\circ\text{C}$ for 6 hours and cooling rate of $3\text{ }^\circ\text{C}/\text{min}$. In the inset is shown a zoom around the structural phase transition towards the HTT phase.

Figure 3 shows thermo-gravimetric analysis (TGA) experiments performed under pure O_2 flowing starting at RT from as prepared $\text{Pr}_2\text{NiO}_{4.22}$. Upon heating up to $750\text{ }^\circ\text{C}$, a weight decrease due to the de-intercalation of interstitial oxygen is observed with δ passing from 0.22 to 0.14. At $T \sim 450\text{ }^\circ\text{C}$ a small step ($\Delta\delta = -0.01$) is detected, which was previously attributed by Allançon *et al.*^{28, 38} to the transition from the “LTO” phase to the HTT phase. Above $750\text{ }^\circ\text{C}$ the decomposition of $\text{Pr}_2\text{NiO}_{4.14}$ into $\text{Pr}_4\text{Ni}_3\text{O}_{10-\delta}$ and PrO_y is evidenced by a significant oxygen uptake as previously

shown by Odier *et al.*³⁸ Upon further heating, such oxygen uptake decreases at 900 °C and is completely lost at 1050 °C. Above this temperature, the observed mass variation corresponds again to the thermal behavior of Pr₂NiO_{4+δ} as followed in the first part of the experiment (500 < T °C < 700), *i.e.*, a slight decrease of delta upon heating. Then, the cooling was performed with a ramp of 3 °C/min corresponding to the one used for the synthesis of the sample; no significant variation is detected apart from a linear increase in weight similar to the mass variation on heating before decomposition.

Taking into account the TGA data and the *ex-situ* laboratory XRPD analyses of the products obtained after TGA, the weight variations in the range between 800 and 1200 °C can be explained as follows: the first oxygen loss at around 900°C results from the conversion of the α phase of PrO_y (y = 1.83) into the ι phase (y = 1.72), in agreement with previous works performed on the praseodymium-oxygen system^{38,39}. For the second abrupt oxygen loss at 1100 °C, although Odier *et al.* ascribed it to the reduction of Pr₄Ni₃O_{9.75} into Pr₄Ni₃O₉ and the conversion of the PrO_y α phase (PrO_{1.83}) to the σ one (PrO_{1.6})³⁸, it should be associated with the recrystallization of Pr₂NiO_{4+δ} (Pr₂NiO_{4.08} for the present experiment) in agreement with Kovalevsky *et al.*⁸. This statement is confirmed by the existence of the reverse small step related to the HTT to “LTO” transition on the cooling curve (inset of Figure 3) and the XRPD analysis of the powder obtained by TGA confirms the recrystallization of Pr₂NiO_{4+δ} (4.22). Finally it is interesting to notice that the recrystallization of Pr₂NiO_{4+δ} (4.22) at 1100 °C is concomitant with the thermodynamic limit of stability of the ι phase of PrO_y.

The cooling behavior of the TGA experiments represented in Figure 3 is very different compared with those of Ref. ³⁸. In the present experiment no major uptake or loss is detected during cooling while in the investigation of Odier *et al.* ³⁸ an important uptake is detected and interpreted by the

formation of $\text{Pr}_4\text{Ni}_3\text{O}_{9.75}$ and $\alpha\text{-PrO}_{1.83}$. At first sight no direct explanation of the two different reactivity behaviors can be given, however it should be stressed that kinetics of the two experiments are very different. The experiment shown in Figure 3 is performed with temperature ramps of 0.5 °C/min for warm up and 3 °C/min for cooling, including a dwell of 6 hours at 1400 °C between the two ramps. Odier *et al.* used ramps of 5 °C/min and practically no dwell between heating and cooling ramps performed till 1150 °C. In order to highlight the role of kinetics on the decomposition reaction, several other TGA experiments have been performed using different heating and cooling rates.

As a matter of fact, as depicted in Figure 4a for the investigated sample, heating at 5 °C/min does not allow decomposing $\text{Pr}_2\text{NiO}_{4.14}$ into $\text{Pr}_4\text{Ni}_3\text{O}_{10-\delta}$ and PrO_y whereas for slower ramps, the decomposition is observed. It is also worth underlining that while the onset of the decomposition reaction is function of the speed of heating, the backward reaction temperature doesn't vary for 0.5 °C/min and 2 °C/min ramps ($T \sim 1100^\circ\text{C}$). On cooling, as it has been previously discussed, a ramp at 3 °C/min is already sufficient to maintain the K_2NiF_4 structure. A significant mass uptake is observed only for a cooling rate of 1 °C/min (blue curve, Figure 4b) . Such uptake has to be ascribed to a partial decomposition of $\text{Pr}_2\text{NiO}_{4+\delta}$ into $\text{Pr}_4\text{Ni}_3\text{O}_{10-\delta}$ and PrO_x as supported by *ex situ* XRPD performed using the sample retrieved from TGA crucible.

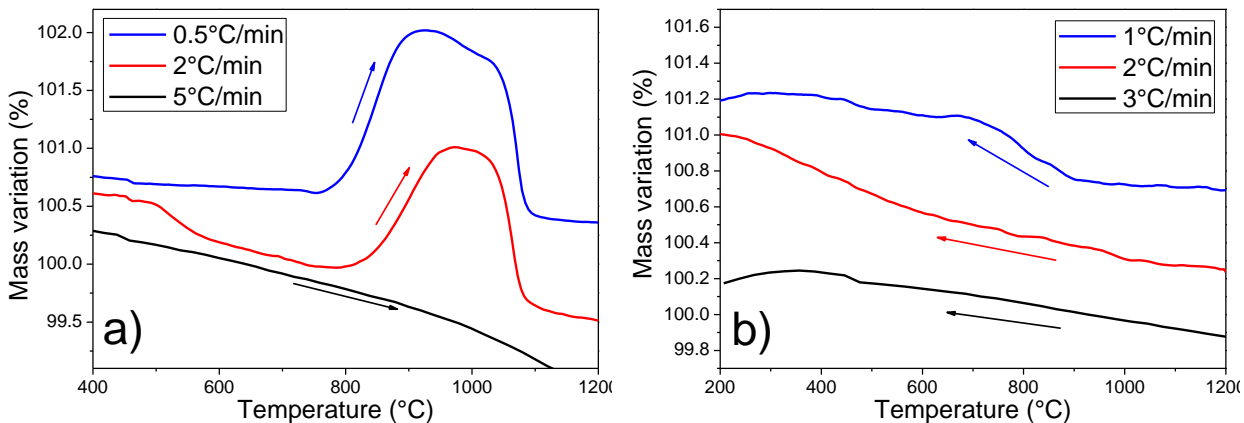


Figure 4. TGA of $\text{Pr}_2\text{NiO}_{4.22}$ performed in O_2 atmosphere using various heating and cooling rates. Part a) and b) represent warming up and cooling, respectively.

To sum up the TGA experiments depicted in Figure 4, the kinetics of the process is a crucial parameter regarding the occurrence of the decomposition process: $3\text{Pr}_2\text{NiO}_{4+\delta} \rightarrow \text{Pr}_4\text{Ni}_3\text{O}_{10-\delta} + 2\text{PrO}_y$. The extreme sensitivity of $\text{Pr}_2\text{NiO}_{4+\delta}$ towards the experimental conditions can explain the differences between the present TGA results and the data of the literature^{8, 9, 38}.

High temperature synchrotron X-ray powder diffraction under O_2

In the temperature range of interest for electrochemical applications, the crystal structure of $\text{Pr}_2\text{NiO}_{4+\delta}$ has been previously probed *in situ* up to 500°C by conventional X-ray diffraction²⁵ and up to 827°C by NPD^{28, 29}. The LTO to HTT phase transition was determined at 417°C in inert atmosphere²⁹, and it was shown to be slightly depend on $p\text{O}_2$ and systematically accompanied by a small oxygen loss ($\Delta\delta \sim 0.01$)²⁵. A structural model was further proposed on the basis of NPD data for the HTT phase at 527°C ($\delta \sim 0.18$; $P4_2/nm$ space group), including a strong degree of anharmonicity for the apical oxygen site²⁸.

In the present study as prepared $\text{Pr}_2\text{NiO}_{4.22}$ heated at 420 °C retains the $F112/m$ monoclinic space group with a small variation of the unit cell parameters: around +0.4% for a and b axes and +0.7% for c axis due to the combined effects of thermal expansion and the partial reduction of Ni^{3+} into Ni^{2+} as observed by TGA, inducing the increase of the ionic radii (0.60 and 0.69 Å for Ni^{2+} and Ni^{3+} , respectively) and the decrease of the Jahn-Teller distortion. The monoclinic angle decreases from $90.066(1)^\circ$ to $90.037(1)^\circ$ and concomitantly the two equatorial oxygen atoms show close isotropic displacement parameters (0.0253(17) and 0.0287(18) Å², respectively).

In order to investigate in details the cell metric variations during the phase transition currently ascribed to the transformation from “LTM” (previously “LTO”) to HTT, the temperature range around the structural transition at 460 °C was monitored by rapid acquisitions over a reduced 2θ range from which two selected regions are shown in Figure 5. HTT (200) reflection is mainly sensitive to the difference between a and b axes (orthorhombic character) while HTT (220) depends on the deviation of γ angle from 90° (monoclinic character). As visible in Figure 5, both orthorhombic and monoclinic characters remain mainly unchanged on heating until the occurrence of the HTT phase around 460 °C. Consequently, it can be stated that the LTM phase transforms directly into the HTT phase and no LTO phase is present in the phase diagram of $\text{Pr}_2\text{NiO}_{4+\delta}$ between RT and the transition to HTT.

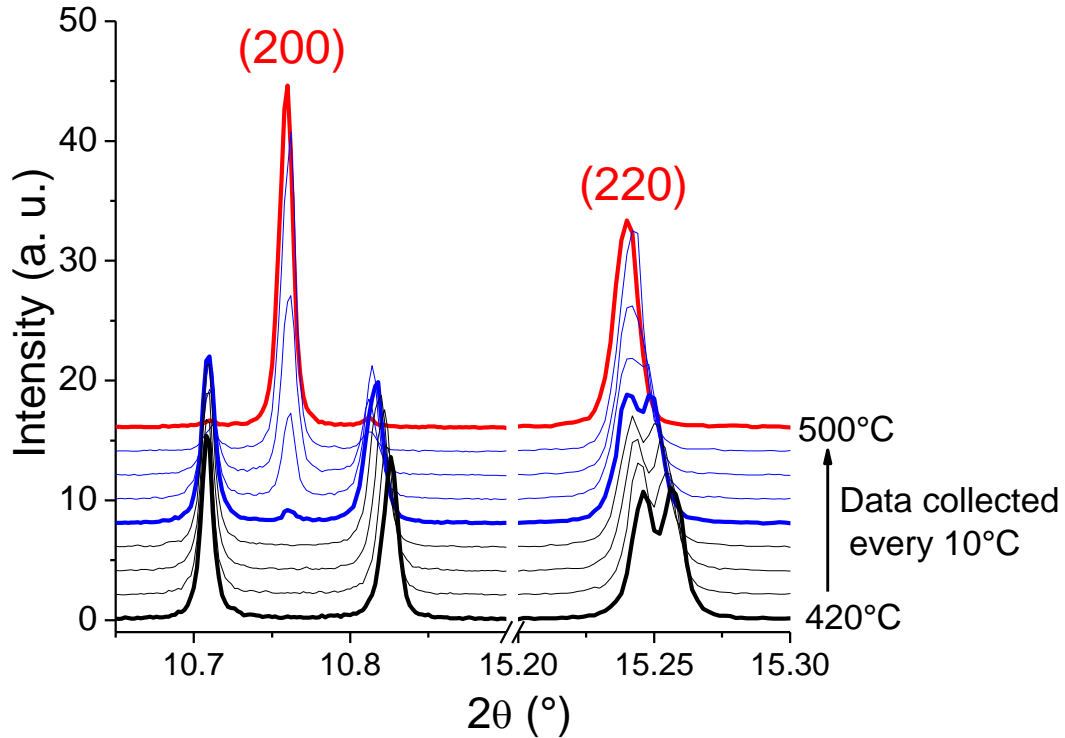


Figure 5. Rapid data collection in O_2 flow from 370 °C to 530 °C focused on the HTT (220) and (200) reflections. LTM phase is represented by black curves, blue curves are used for phase coexistence while red curve corresponds to the HTT phase.

At 480 °C, the unit cell is fully tetragonal and all the reflections can be indexed within the $F4/mmm$ space group. The absence of the weak superstructure peaks associated with the $P4_2/nm$ space group²⁸ as detected by NPD at 527 °C could be again related either to kinetics factor or to the lower sensitivity of X-ray diffraction to oxygen. No lattice expansion is detected compared to the LTM phase at 450 °C, the cell parameter c remains unchanged and a_{HTT} is equal to the average between a_{LTM} and b_{LTM} . By analogy with the study of $La_2NiO_{4+\delta}$ ²¹, the increase of symmetry occurring at the LTM to HTT phase transition can be basically ascribed to the complete loss of coherence of NiO_6 octahedra positions due to their dynamically activated tilts. The HTT phase remains stable up to 600 °C with only a minor expansion and an expected general increase of the ADPs.

Patterns collected at 480 °C and 600 °C still show unindexed peaks either using the $F4/mmm$ or the $P4_2/nm$ space groups. Once again those unindexed peaks would suggest the presence of an incommensurate structural modulation surviving (and evolving, see below) even at high temperature.

At 800 °C shoulders occur on all the reflections at lower angles side, as shown in Figure 6 for reflections (113) and (200). Such shoulders are assigned to another tetragonal $F4/mmm$ phase with slightly larger cell parameters. This phase separation of $\text{Pr}_2\text{NiO}_{4+\delta}$ at high temperature is a reversible phenomenon: at decreasing temperature down to 480 °C, it is noticed that a single HTT phase is recovered (red curve in Figure 6).

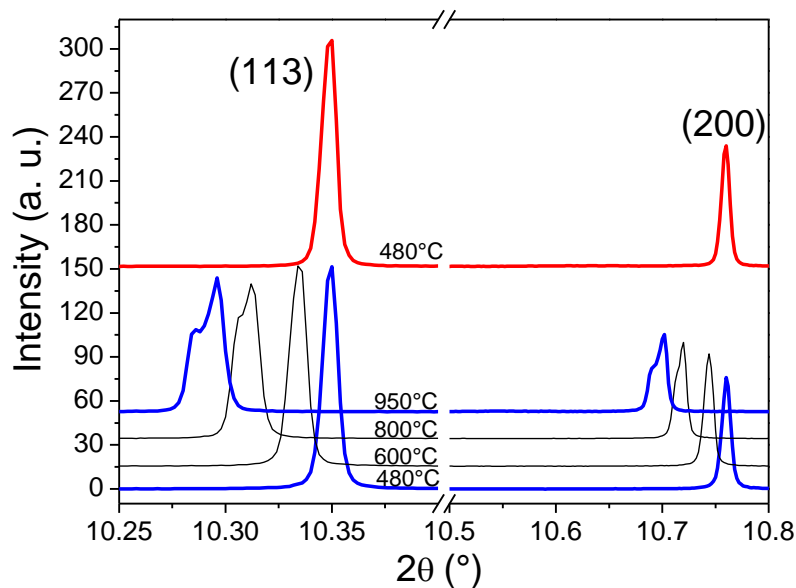


Figure 6. Reflections (113) and (200) showing the split of each individual reflection for $T \geq 800$ °C. The top pattern (red curve) corresponds to the material cooled back to 480 °C after the high temperature phase separation.

The small difference in the cell parameters between the two coexisting HTT phases (+0.06% along a and +0.05% along c) as well as the reversibility of the phase segregation suggest that this difference in cell parameters could be due to a slight difference in interstitial oxygen

occupancy. Indeed it is well known that the volume of K_2NiF_4 type oxides is correlated with oxygen stoichiometry⁴⁰.

41.

Two-phase Rietveld refinement of the high resolution patterns collected at 800, 900 and 950 °C supports the coexistence of two K_2NiF_4 tetragonal phases (\approx 63% and 37%, weight fractions). However refinement of interstitial oxygen occupancy leads to unstable and non-reproducible values. Indeed, in the present case, the unit cell parameters are so close that the overlapping of the reflection of the two phases is almost total, as a consequence small variation in the deconvolution of the peaks strongly affects the intensity estimation of reflection for each phase.

As stressed in the thermo-gravimetric analysis section, the decomposition of $Pr_2NiO_{4+\delta}$ into $Pr_4Ni_3O_{10-\delta} + 2PrO_y$ is highly dependent on the kinetics of the process, which could shift this decomposition at higher temperatures or even totally suppress it. During *in-situ* synchrotron XRPD experiments, the temperature was increased step by step to keep the temperature constant for each measurement. Such a procedure corresponds to a relatively fast heating ramp, although not directly comparable with the heating ramp used during TGA experiment. As a consequence, only a very minor decomposition into $Pr_4Ni_3O_{10-\delta}$ and PrO_y (estimated by Rietveld refinement to 2.5 % wt and 1.2 % wt, respectively) was observed above 900°C.

Influence of the oxygen partial pressure

The influence of the oxygen partial pressure on the phase decomposition reaction during the synchrotron XRPD experiments has been investigated using two different pO_2 : pure O_2 and Ar. As far as it could be observed, the pO_2 atmosphere has no drastic effect on highly crystalline $Pr_2NiO_{4.22}$. The main variations consist in a small shift in the lattice parameters and a slightly different proportion of the two HTT coexisting phases. This probably reflects the lack of reactivity *versus* O_2 gas of the large particle of solid-state synthesized powder. As an illustration the patterns collected at 900 °C under pure O_2 and Ar, respectively, are compared in Figure 7.

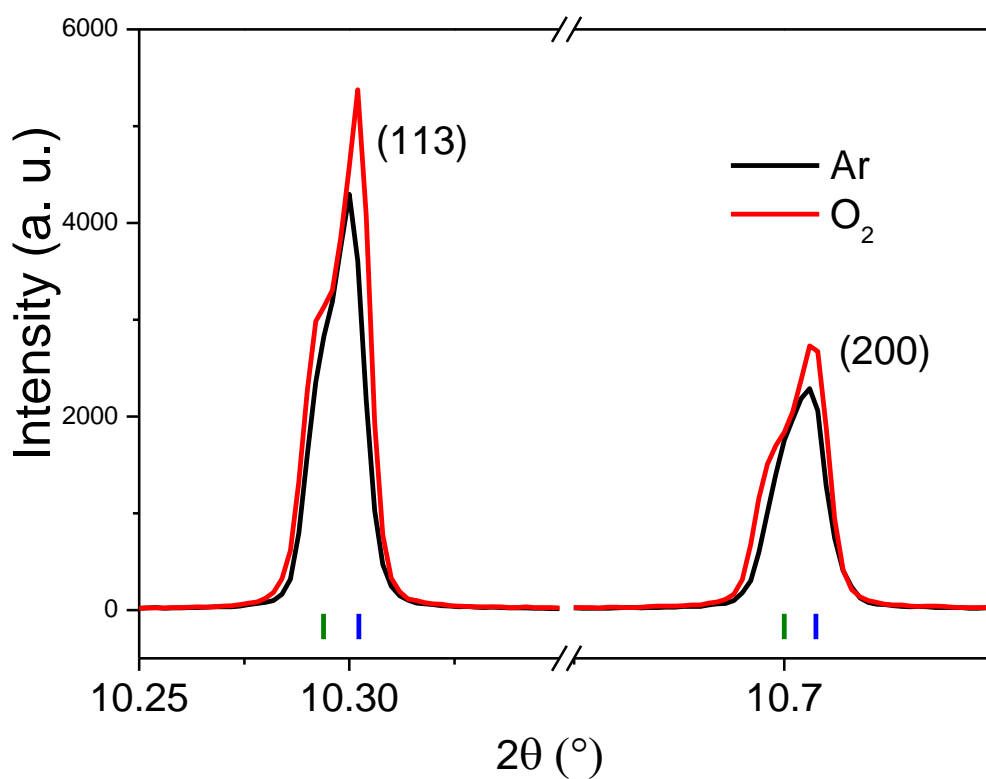


Figure 7. Raw data comparison of $Pr_2NiO_{4.22}$ at 900°C in argon (black) and oxygen (red). Green and blue ticks highlight the two coexisting HTT phases.

Temperature dependent structural modulations

Using long wavelength NPD data ($\lambda = 2.52 \text{ \AA}$), Fernández-Diaz *et al.* revealed that $\text{PrNiO}_{4.2(1)}$ exhibits at RT a more complex crystal structure than orthorhombic *Bmab* (only based on the intensity of the main reflections) as testified by the presence of super-lattice reflections but no structure determination was attempted²⁹. The presence of unindexed super-lattice reflections has been confirmed by Sullivan *et al.* by XRPD³⁰ although a *Fmmm* average symmetry was assigned to high- δ compounds.

As previously discussed, those few unindexed peaks already observed at RT could be ascribed to a structural modulation probably related with possible arrangements of octahedra tilt and/or occupational ordering of interstitial oxygen atoms. Figure 8 shows the thermal evolution from RT to 900 °C of some selected satellite reflections for $\text{Pr}_2\text{NiO}_{4+\delta}$ under oxygen. The low intensity and the limited number of observable satellite peaks (only around ten emerge from the background) associated with the expected complexity as the presence of more than one modulation vector (according to what was found for homologous $\text{La}_2\text{CoO}_{4.14}$ ³²) does not allow as underlined above the success of a modulation vector indexing routine. These unindexed peaks must not be ascribed to impurity ones, indeed they are strongly related with the thermal phase evolution of $\text{Pr}_2\text{NiO}_{4+\delta}$:

- i) they change concomitantly with the observed structural transitions;

ii) at 900 °C, satellites are also doubled due to the presence of two $\text{Pr}_2\text{NiO}_{4+\delta}$ HTT coexisting phases associated to two very close δ values.

It is worthwhile to underline that the persistence of the satellites up to temperatures as high as 900 °C is quite surprising. Indeed at such a high temperature the interstitial oxygen network should be totally disordered due to the high ionic diffusivity in these phases. Consequently, for $\text{Pr}_2\text{NiO}_{4+\delta}$ a pure interstitial oxygen occupational modulation should be discarded and a more complex modulated structure must be considered.

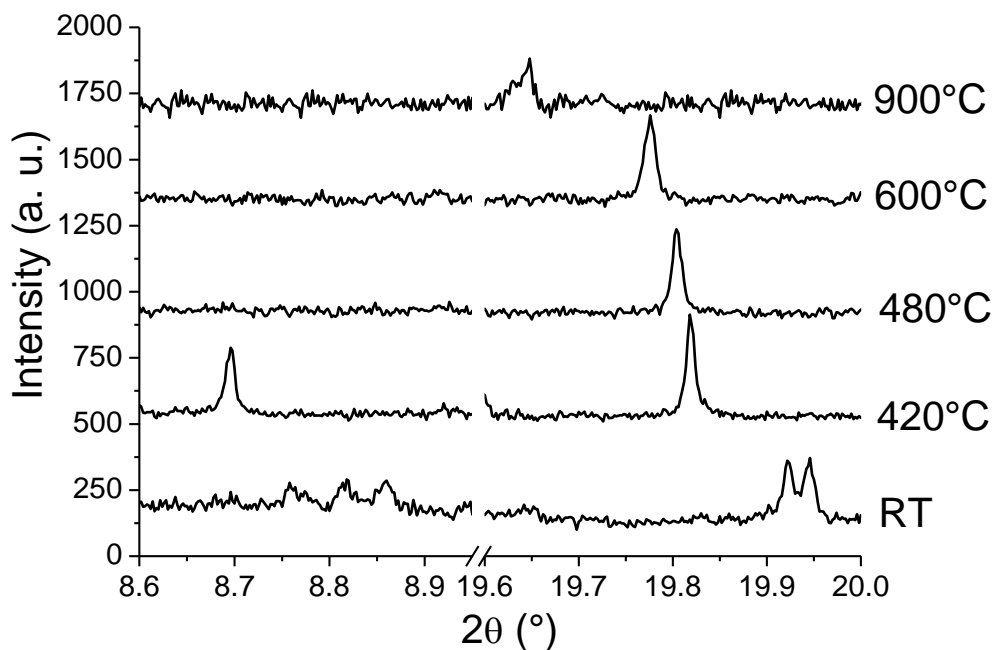


Figure 8. Thermal evolution under O_2 of few observable satellite reflections at RT, 420, 480, 600 and 900 °C.

A complex structural modulation has recently been reported in a K_2NiF_4 -type structure for $\text{La}_2\text{CoO}_{4+\delta}$. Structural modulations observed by synchrotron X-ray single-crystal diffraction are temperature and oxygen content dependent in a complex way³². Moreover, previous NPD study on

$\text{Pr}_2\text{NiO}_{4+\delta}$ ²⁸ assigned the unindexed peaks (still present up to 417 °C) in the *Bmab* space group to incommensurate modulation due to oxygen interstitial order. The real incommensurate structure of both latter important and archetypical K_2NiF_4 oxides still remain to be solved and refined through the superspace group approach.

Conclusion

A high resolution synchrotron XRPD study of $\text{Pr}_2\text{NiO}_{4+\delta}$ as a function of temperature and oxygen partial pressure, complemented by TGA experiments, is reported. For $\text{Pr}_2\text{NiO}_{4.22}$, a monoclinic symmetry is evidenced from RT to 460 °C and the structure refined accordingly to a long range disordered tilt of NiO_6 octahedra along both [100] and [110] directions. Such a monoclinic phase should therefore substitute at least above RT the so far called “Low Temperature Orthorhombic” phase in the phase diagram of $\text{Pr}_2\text{NiO}_{4.22}$. Further investigations will be necessary to figure out whether such statements could be extended starting at RT from oxygen stoichiometries lower than 4.22.

The structure of $\text{Pr}_2\text{NiO}_{4.22}$ is incommensurately modulated at RT and all the structural descriptions previously proposed, including that of the present work, should be considered as incomplete since they represent only the average structure; the real structure still remains to be determined in the superspace description. Surprisingly, even at high temperature (up to 900 °C) $\text{Pr}_2\text{NiO}_{4+\delta}$ remains modulated although modulation vector modifies as a function of the temperature.

Controversies encountered in the literature about decomposition reaction $3\text{Pr}_2\text{NiO}_{4+\delta} \rightarrow \text{Pr}_4\text{Ni}_3\text{O}_{10-\delta} + 2\text{PrO}_y$ should be contextualized following the high sensitivity of this reaction with respect to the experimental conditions. In this study ramp rate is investigated, but we could expect that other parameters such as sample morphology or gas flow should play a role, as previously mentioned by Odier *et al.*³⁸.

In order to elucidate in more details the real modulated structure of $\text{Pr}_2\text{NiO}_{4+\delta}$ (including its thermal evolution) and to more deeply understand its interplay with ionic conductivity observed in this important SOFC cathode material, *in-situ* single crystal studies must be carried out.

Author information

Olivier.Hernandez@univ-rennes1.fr

Carmelo.Prestipino@univ-rennes1.fr

Institut des Sciences Chimiques de Rennes, UMR N°6226 CNRS-Université de Rennes 1
Campus de Beaulieu, 263 avenue du Général Leclerc F-35042 RENNES (France)

References

1. Liu, Y. L.; Hagen, A.; Barfod, R.; Chen, M.; Wang, H. J.; Poulsen, F. W.; Hendriksen, P. V., *Solid State Ionics* **2009**, *180*, 1298-1304.
2. Yokokawa, H.; Horita, T.; Sakai, N.; Yamaji, K.; Brito, M. E.; Xiong, Y. P.; Kishimoto, H., *Solid State Ionics* **2006**, *177*, 3193-3198.
3. Jiang, S., *J Mater Sci* **2008**, *43*, 6799-6833.
4. Jacobson, A. J., *Chem. Mater.* **2010**, *22*, 660-674.
5. V. Kharton, V.; P. Viskup, A.; N. Naumovich, E.; M. B. Marques, F., *J. Mater. Chem.* **1999**, *9*, 2623-2629.
6. Kharton, V. V.; Viskup, A. P.; Kovalevsky, A. V.; Naumovich, E. N.; Marques, F. M. B., *Solid State Ionics* **2001**, *143*, 337-353.
7. Yashima, M.; Sirikanda, N.; Ishihara, T., *J. Am. Chem. Soc.* **2010**, *132*, 2385-2392.
8. Kovalevsky, A. V.; Kharton, V. V.; Yaremchenko, A. A.; Pivak, Y. V.; Tsipis, E. V.; Yakovlev, S. O.; Markov, A. A.; Naumovich, E. N.; Frade, J. R., *J. Electroceram.* **2007**, *18*, 205-218.
9. Kovalevsky, A. V.; Kharton, V. V.; Yaremchenko, A. A.; Pivak, Y. V.; Naumovich, E. N.; Frade, J. R., *J. Eur. Ceram. Soc.* **2007**, *27*, 4269-4272.
10. Steele, B., *Solid State Ionics* **2000**, *129*, 95-110.
11. Fergus, J. W., *J. Power Sources* **2006**, *162*, 30-40.
12. Ferchaud, C.; Grenier, J.-C.; Zhang-Steenwinkel, Y.; van Tuel, M. M. A.; van Berkel, F. P. F.; Bassat, J.-M., *J. Power Sources* **2011**, *196*, 1872-1879.
13. Yashima, M., *J. Ceram. Soc. Jpn.* **2009**, *117*, 1055-1059.
14. Yashima, M.; Enoki, M.; Wakita, T.; Ali, R.; Matsushita, Y.; Izumi, F.; Ishihara, T., *J. Am. Chem. Soc.* **2008**, *130*, 2762-2763.
15. Parfitt, D.; Chronos, A.; Kilner, J. A.; Grimes, R. W., *PCCP* **2010**, *12*, 6834-6836.
16. Andersen, I. G. K.; Andersen, E. K.; Norby, P.; Skou, E., *J. Solid State Chem.* **1994**, *113*, 320-326.
17. Izumi, F.; Momma, K., *Solid State Phenom.* **2007**, *130*, 15-20.
18. Ida, T., *J. Appl. Crystallogr.* **2010**, *43*, 1124-1125.
19. Rodriguezcarvajal, J., *Physica B* **1993**, *192*, 55-69.
20. Stephens, P. W., *J. Appl. Crystallogr.* **1999**, *32*, 281-289.
21. Rodriguez-Carvajal, J.; Fernandez-Diaz, M.; Martinez, J., *J. Phys.: Condens. Matter* **1991**, *3*, 3215.
22. Willer, B.; Daire, M., *C.R. Acad. Sci., Ser. IIC: Chim.* **1968**, *267*, 1482-&.
23. Singh, K. K.; Ganguly, P.; Goodenough, J. B., *J. Solid State Chem.* **1984**, *52*, 254-273.
24. Ganguly, P.; Rao, C. N. R., *J. Solid State Chem.* **1984**, *53*, 193-216.
25. Allançon, C.; Gonthier-Vassal, A.; Bassat, J. M.; Loup, J. P.; Odier, P., *Solid State Ionics* **1994**, *74*, 239-248.

26. Saez Puche, R.; Fernandez, F.; Rodríguez Carvajal, J.; Martinez, J., *Solid State Commun.* **1989**, *72*, 273-277.
27. Fernandez-Diaz, M.; Rodríguez-Carvajal, J.; Martinez, J.; Fillion, G.; Fernandez, F.; Saez-Puche, R., *Z. Phys. B: Condens. Matter* **1991**, *82*, 275-282.
28. Allançon, C.; Rodriguez-Carvajal, J.; Fernández-Diaz, M. T.; Odier, P.; Bassat, J. M.; Loup, J. P.; Martinez, J. L., *Z. Phys. B: Condens. Matter* **1996**, *100*, 85-90.
29. Fernández-Díaz, M.; Martínez, J.; Rodríguez-Carvajal, J., *Solid State Ionics* **1993**, *63*, 902-906.
30. Sullivan, J. D.; Buttrey, D. J.; Cox, D. E.; Hriljac, J., *J. Solid State Chem.* **1991**, *94*, 337-351.
31. Le Toquin, R.; Paulus, W.; Cousson, A.; Dhahlenne, G.; Revcolevschi, A., *Physica B* **2004**, *350*, E269-E272.
32. Le Dreau, L.; Prestipino, C.; Hernandez, O.; Schefer, J.; Vaughan, G.; Paofai, S.; Perez-Mato, J. M.; Hosoya, S.; Paulus, W., *Inorg. Chem.* **2012**, *51*, 9789-9798.
33. Moret, R.; Pouget, J. P.; Collin, G., *Europhys. Lett.* **1987**, *4*, 365.
34. Demourgues, A.; Weill, F.; Darriet, B.; Wattiaux, A.; Grenier, J. C.; Gravereau, P.; Pouchard, M., *J. Solid State Chem.* **1993**, *106*, 317-329.
35. Radaelli, P.; Hinks, D.; Mitchell, A.; Hunter, B.; Wagner, J.; Dabrowski, B.; Vandervoort, K.; Viswanathan, H.; Jorgensen, J., *Phys. Rev. B: Condens. Matter* **1994**, *49*, 4163.
36. Frayret, C.; Villesuzanne, A.; Pouchard, M., *Chem. Mater.* **2005**, *17*, 6538-6544.
37. Aspera, S.; Sakaue, M.; Wungu, T.; Alaydrus, M.; Linh, T.; Kasai, H.; Nakanishi, M.; Ishihara, T., *J. Phys.: Condens. Matter* **2012**, *24*, 405504.
38. Odier, P.; Allançon, C.; Bassat, J. M., *J. Solid State Chem.* **2000**, *153*, 381-385.
39. Hyde, B.; Bevan, D.; Eyring, L., *Philos. Trans. R. Soc. London, Ser. A* **1966**, *259*, 583-614.
40. Nakamura, T.; Yashiro, K.; Sato, K.; Mizusaki, J., *Solid State Ionics* **2010**, *181*, 402-411.
41. Nakamura, T.; Yashiro, K.; Sato, K.; Mizusaki, J., *Solid State Ionics* **2010**, *181*, 292-299.

For Table of Contents Only

The high temperature behaviour of the SOFC cathode material $\text{Pr}_2\text{NiO}_{4+\delta}$ is revisited by *in situ* synchrotron XRPD experiments under O_2 . Its crystal structure, that turns out to be monoclinic and incommensurately modulated already at RT, directly transforms to the HTT phase at 480 °C. Above 800 °C an unexpected reversible phase segregation is observed. The incommensurate modulation is surviving up to at least 950 °C. The role of kinetics on the decomposition process is highlighted through new TGAs experiments.

For Table of Contents Only: Graphic

